Can we approach the gas–liquid critical point using slab simulations of two coexisting phases?

Florent Goujon,[1] Aziz Ghoufi,[2] Patrice Malfreyt,[1,a)] and Dominic J. Tildesley[3]
[1]*Clermont Université, Université Blaise Pascal, Institut de Chimie de Clermont-Ferrand, ICCF, UMR CNRS 6296, BP 10448, F-63000 Clermont-Ferrand, France*
[2]*Institut de Physique de Rennes, UMR CNRS 6251, Université Rennes 1, 263 Avenue du Général Leclerc, 35042 Rennes, France*
[3]*EPFL-CECAM, Batochime (BCH), CH-1015 Lausanne, Switzerland*

(Received 27 May 2016; accepted 2 September 2016; published online 23 September 2016)

In this paper, we demonstrate that it is possible to approach the gas–liquid critical point of the Lennard-Jones fluid by performing simulations in a slab geometry using a cut-off potential. In the slab simulation geometry, it is essential to apply an accurate tail correction to the potential energy, applied during the course of the simulation, to study the properties of states close to the critical point. Using the Janeček slab-based method developed for two-phase Monte Carlo simulations [J. Janeček, J. Chem. Phys. **131**, 6264 (2006)], the coexisting densities and surface tension in the critical region are reported as a function of the cutoff distance in the intermolecular potential. The results obtained using slab simulations are compared with those obtained using grand canonical Monte Carlo simulations of isotropic systems and the finite-size scaling techniques. There is a good agreement between these two approaches. The two-phase simulations can be used in approaching the critical point for temperatures up to 0.97 T_C^* ($T^* = 1.26$). The critical-point exponents describing the dependence of the density, surface tension, and interfacial thickness on the temperature are calculated near the critical point. *Published by AIP Publishing.* [http://dx.doi.org/10.1063/1.4962820]

I. INTRODUCTION

Over the last 40 years, the surface tension of the Lennard-Jones (LJ) fluid has been thoroughly investigated using molecular simulations in the slab geometry.[1–17] The strong gradients in the density across the periodic simulation cell mean that many of the approximations commonly used in simulations of isotropic systems are no longer valid. In particular, the calculation of the surface tension is sensitive to a number of factors including: the system-size,[16,18–22] the size of the box parallel and perpendicular to the interface, the range of the interatomic interactions,[7,21,23] the truncation of the potential,[7,24] the mechanical and thermodynamic definitions used for the calculation of the surface tension,[9,24,25] the long-range corrections to be applied to both the surface tension[6,10,24,26–30] and the configurational energy.[6,10,30,31] A number of recommendations addressing these issues have been summarised in a recent review[17] and we are now in a position to make an accurate calculation for the surface tension along most of the orthobaric curve of a simple model fluid.

It has been shown that the slab-based tail methods developed by Guo and Lu[6] and Janeček,[10] that add a local tail correction to the configurational energy at each step of the simulation perform, are accurate for the calculation of the surface tension of a variety of atomic and molecular fluids.[12–14,17] In addition, we have shown[16] that both methods produce the same results within the estimated error. Since the method of Janeček involves almost no additional computational overhead, we have used it extensively for temperatures away from the critical point.[16] Both methods avoid any cutoff-dependence for the surface tension for $r_c > 3.0\,\sigma$. As an example, the liquid density and surface tension of the LJ fluid calculated at $T^* = 0.84$ (i.e., $\approx 0.65\,T_C^*$) using the Janeček method are shown in Fig. 1 as a function of r_c.[16] The use of slab-based tail methods[10,16,31] leads to simulated densities and surface tensions that are independent of r_c within relative deviations of less than 1% for temperatures less than $0.85\,T_C^*$, where T_C^* is the reduced critical temperature. To achieve the same accuracy in the calculation of the surface tension and coexisting densities with the truncated LJ potential using no long range corrections in the Markov chain, but where we attempt to add the correction at the end of the simulation, requires a cutoff of $5.0\,\sigma$.

For temperatures greater than $0.85\,T_C^*$, the situation is much less clear since the two-phase simulations have not been used to explore the critical region. Actually, as the temperature approaches the critical temperature ($T^* > 0.9\,T_C^*$), the two-phase simulations must be carried out with care due to the difficulty of stabilizing the interface. The absence of a stable interface in simulations with explicit interfaces prevents any calculation of the surface tension. Alternative methodologies for calculating the surface tension[32–34] in the critical region avoid an explicit interface. For example, the combination of grand canonical Monte Carlo simulations with the finite-size scaling methodology developed by Binder[35] has been used to predict the surface tension[33] of the LJ fluid for a range of reduced temperature $T^* = 0.95 - 1.31$. Although

a)Patrice.Malfreyt@univ-bpclermont.fr

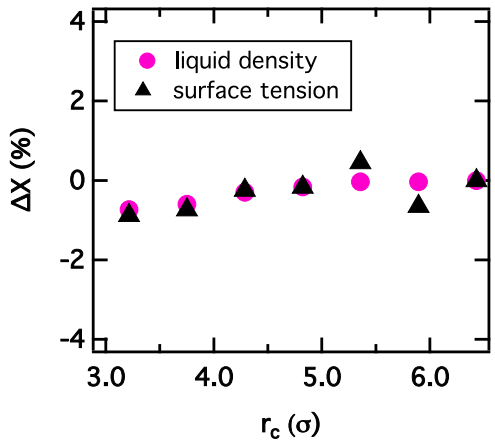

FIG. 1. $\Delta X = 100 * \left[X(r_c) - X(r_{c,full})\right] / X(r_{c,full})$; the relative deviation calculated for the liquid density and surface tension at $T^* = 0.84$ where $r_{c,full} = 6.43\,\sigma$.

this approach is useful in the critical region, it does not work for lower temperatures ($T^* < 0.7\,T_C^*$) as the free energy barriers between the coexisting liquid and vapor phases becomes too large to explore both phases in a simulation of a reasonable length. This approach has been considered as a complementary method to the slab simulations that provide the opportunity to study the whole orthobaric curve from triple to critical point. The surface tensions calculated by Potoff and Panagiotopoulos[33] will be used for the comparison with those calculated in the slab geometry. Intensive Gibbs Ensemble Monte Carlo (GEMC) simulations[36] have also been performed recently on large system-sizes to investigate the cutoff-dependence of the coexisting densities of the LJ fluid in the near-critical region.

Errington[34] has also proposed a method that can be applied over the entire liquid-vapor phase envelope. This approach is based on the use of the transition matrix technique[37] in a grand canonical ensemble. The surface tension is then calculated by the finite-size scaling of Binder.[35] The method has been tested over a range of reduced temperature $T^* = 0.70 - 1.31$, where the reduced critical temperature T_C^* was estimated at 1.31.

Parallel Monte Carlo codes can perform slab simulations including the explicit tail corrections at each step, rapidly. A typical parallel MC simulation carried out over 6 processors lasts from 3 days to 9 days depending on the cutoff and temperature. At a given cutoff, simulations at $T^* = 1.28$ are 30% shorter than the simulations at $T^* = 1.10$ due to a lower density in the liquid phase.

In this paper, we address the question of whether it is possible to extend slab simulations of vapor-liquid coexistence into the critical region. We analyse the cut-off dependence of the results and the use of Janeček correction close to T_C. The results are compared with the corresponding grand canonical simulation results. The outline of this paper is as follows. In Sec. II, we present the interaction potential used within the Janeček methodology and we describe the calculation of the surface tension and of its long range correction due to the truncation of the potential. Sec. III presents the main results concerning the cutoff-dependence of the coexisting densities and surface tensions calculated with the Janeček method in the critical region and some recommendations on how to perform these calculations. The main conclusions of this work are given in Sec. IV.

II. SIMULATION METHODOLOGY

A. Potential model

In the Janeček approach, a long-range correction to the truncated potential is added to the truncated $u_{ST}(r_{ij})$ potential. Considering a system of N atoms, the total configurational energy U_{TOT} is

$$U_{TOT} = \sum_{i=1}^{N-1} \sum_{j=i+1}^{N} u_{ST}(r_{ij}) + U_{LRC}, \tag{1}$$

where r_{ij} is the pair separation distance and $u_{ST}(r_{ij})$ is the spherically truncated Lennard-Jones potential defined by

$$u_{ST}(r_{ij}) = \begin{cases} u_{LJ}(r_{ij}) & r_{ij} < r_c \\ 0 & r_{ij} \geq r_c \,. \end{cases} \tag{2}$$

u_{LJ} is the Lennard-Jones (LJ) potential defined by ϵ and σ corresponding to energy and size parameters, respectively. The simulation box is divided into N_s slabs of width Δz. Each slab, which is parallel to the interface, has a volume $V_s = L_x L_y \Delta z$ and z_k defines the centre of the kth slab. In Eq. (1), U_{LRC} is defined as

$$U_{LRC} = \frac{1}{2} \sum_{k=1}^{N_s} u_{lrc}(z_k), \tag{3}$$

where the long-range correction energy of the slab k is

$$u_{lrc}(z_k) = \rho(z_k) V_s \sum_{j=1}^{N_s} \rho(z_j) w(|z_j - z_k|) \Delta z, \tag{4}$$

where the sum is over all the slabs in the box. $\rho(z_k)$ defines the density number of the slab k. The contribution $w(\xi) = w(|z_j - z_k|)$ is calculated by assuming a uniform distribution of atoms in the slab. For the Lennard-Jones potential, the function $w(\xi)$ is

$$w(\xi) = \begin{cases} 4\pi\epsilon\sigma^2 \left[\frac{1}{5} \left(\frac{\sigma}{r_c} \right)^{10} - \frac{1}{2} \left(\frac{\sigma}{r_c} \right)^{4} \right] & \text{for } \xi \leq r_c \\ 4\pi\epsilon\sigma^2 \left[\frac{1}{5} \left(\frac{\sigma}{\xi} \right)^{10} - \frac{1}{2} \left(\frac{\sigma}{\xi} \right)^{4} \right] & \text{for } \xi > r_c \end{cases} . \tag{5}$$

B. Surface tension

The intrinsic part of the surface tension, γ_I, calculated using the Irving and Kirkwood[38–43] definition, uses the components $p_N(z)$ and $p_T(z)$ of the pressure tensor as a function of z,

$$\gamma_I = \int_{-L_z/2}^{L_z/2} \Big(p_N(z) - p_T(z) \Big) dz. \tag{6}$$

Eq. (6) is a mechanical definition of γ based upon the force acting across a unit area in the z-plane for one interface. There is no unique way of calculating the forces across a particular area, since it is unclear which atoms contribute to this force. This has no effect on $p_N(z)$ but different choices of the contour can affect the definition of $p_T(z)$. However, these choices have no effect on the integral in Eq. (6). A typical choice of contour[40,41] due to Irving and Kirkwood gives

$$p_{\alpha\beta}(z) = \langle\rho(z)\rangle k_B T \mathbf{I} + \frac{1}{A}\left\langle \sum_{i=1}^{N-1}\sum_{j=i+1}^{N} (\mathbf{r_{ij}})_\alpha (\mathbf{f_{ij}})_\beta \frac{1}{|z_{ij}|} \times \theta\left(\frac{z-z_i}{z_{ij}}\right)\theta\left(\frac{z_j-z}{z_{ij}}\right)\right\rangle, \quad (7)$$

where $\mathbf{I}$ is the unit tensor, $\theta(x)$ is the unit step function defined as $\theta(x) = 0$ when $x < 0$ and $\theta(x) = 1$ when $x \geq 0$. A is the surface area and $\rho(z)$ is the local number density. The simulation in box is divided into N_z slabs of thickness Δz. Following Irving and Kirkwood, atoms i and j provide a contribution to the pressure tensor in a given slab if the line joining their centres crosses, starts, or finishes in the slab. The contribution to a particular slab is $\Delta/|z_{ij}|$ of the ij interaction. The advantage of the IK approach is that the profile of $p_N(z)$ is a constant for mechanical stability and combined with the symmetry of $p_T(z)$ around both interfaces provides a useful check of the accuracy of the simulation.

Due to the truncation of the potential, the long range corrections to the surface tension are calculated with the Janeček approach as

$$\gamma_{\text{lrc}}(z_k) = \frac{V_s}{A}\left[p_{\text{N,lrc}}(z_k) - p_{\text{T,lrc}}(z_k)\right], \quad (8)$$

where the normal and tangential components of the long-range corrections of the pressure tensor are given by

$$p_{\text{N,lrc}}(z_k) = \rho(z_k)\sum_{j=1}^{N_s}\rho(z_j)\pi_{zz}(|z_j - z_k|)\Delta z \quad (9)$$

and

$$p_{\text{T,lrc}}(z_k) = \frac{1}{2}\left(p_{xx,\text{lrc}}(z_k) + p_{yy,\text{lrc}}(z_k)\right) = \rho(z_k)\sum_{j=1}^{N_s}\rho(z_j)\frac{1}{2}\left(\pi_{xx}(|z_j - z_k|) + \pi_{yy}(|z_j - z_k|)\right)\Delta z \quad (10)$$

(see Ref. 16 for completeness). The total long-range correction γ_{LRC} to the surface tension using the Janeček methodology is then calculated by summing up the local contributions $\gamma_{\text{lrc}}(z_k)$ of each bin and dividing the result γ_{LRC} by a factor of 2 to account for the two planar interfaces in the box.

C. Monte Carlo simulations

The results of the simulations are reported as reduced quantities,[44] where $T^* = k_B T/\epsilon$, $\gamma^* = \gamma\sigma^2/\epsilon$, $L^* = L/\sigma$, $p^* = p\sigma^3/\epsilon$, $\rho^* = \rho\sigma^3$, where $T^*, \gamma^*, L^*, p^*, \rho^*$ represent the reduced temperature, surface tension, length, pressure, and density, respectively.

The initial configuration was constructed by placing N atoms in an orthorhombic box of $L_x^* = L_y^* = 13.4$ and $L_z^* = 35$. The number of atoms is $N = 5000$. MC simulations in the constant-NPT ensemble were performed on this single phase liquid configuration. The dimension of the initial box was increased along the z axis by placing two empty cells on either side of the original box. The resulting two-phase simulation box was rectangular with a volume $V = L_x L_y L_z$ and an interfacial area defined by $A = L_x L_y$. The periodic boundary conditions were applied to the extended box in all three directions. The dimensions of the cell are $L_x^* = L_y^* = 13.4$ while $L_z^* = 93.8$.

MC simulations were performed in the constant-NVT ensemble. All simulations were organized in cycles. Each cycle consisted of N translations. The equilibration phase was composed of 500 000 cycles and the production phase of 2×10^6 cycles (10^{10} translation moves). The maximum displacement was adjusted during the equilibrium phase to give an acceptance ratio of 0.4. The thermodynamic and mechanical properties were calculated every 20 cycles requiring the storage of 100 000 configurations. The statistical errors for these properties were estimated using 5 superblocks averages of 20 000 configurations. For the calculation of the density, pressure, and surface tension profiles, we take care to place the center of the liquid phase at the center of the simulation box for each saved configuration. In doing so, the positions of the Gibbs diving surfaces are updated every 10 saved configurations by using the tangent hyperbolic function for fitting the density profile.

The long-range corrections to the energy are applied at each MC move although the density profile used to calculate the long-range corrections is updated every 10 MC cycles.[30] The MC calculations were carried out at different reduced temperatures ranging from 1.10 to 1.26 for cutoff radius r_c^* changing from 3.2 to 4.8 and from 1.10 to 1.28 for the largest cutoff radius $r_c^* = 6.43$ used in this work. Typical equilibrium configurations of the liquid-vapor LJ fluid are given for $T^* = 1.10$ and 1.23 in Fig. 2.

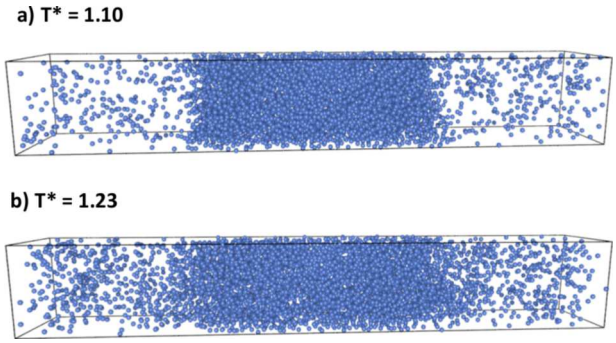

FIG. 2. Typical configurations of the liquid-vapor interface of the Lennard-Jones fluid at two reduced temperatures $T^* = 1.10$ and $T^* = 1.23$.

III. RESULTS AND DISCUSSIONS

We investigate the critical region by studying temperatures greater than 0.85 T_C^* (i.e., $T^* > 1.1$). The density profiles of Fig. 3(a) are calculated from MC simulations using the Janeček approach with a reduced cutoff radius of $r_c^* = 6.43$ at different temperatures ranging from 1.10 to 1.28. Fig. 3(a) shows the superimposition of the left-hand and right-hand sides of $\rho^*(z^*)$. We observe that the density profiles are well-developed leading to stable bulk phases with a well-delimited interfacial region. It is less true for $\rho^*(z^*)$ at $T^* = 1.28$ where the density in the liquid phase is much less flat. Whereas for $T^* < 1.28$, the two sides of the density profiles are symmetrical, some differences between the two sides appear at the interface for $T^* = 1.28$.

These density profiles are then fitted to a hyperbolic tangent function[12–14] in order to obtain the coexisting densities and a parameter d^* related to the thickness of the interface. The thickness of the interface is then represented in Fig. 3(b) at different temperatures. We observe a gradual increase of the thickness in the [1.10–1.28] temperature range and an abrupt change from $T^* = 1.28$. In light of these profiles, we can conclude that the calculation of the coexisting liquid and vapor densities from two-phase simulations is possible in the critical region up to a limit reduced temperature of 1.26 when a cutoff of $r_c^* = 6.43$ is used.

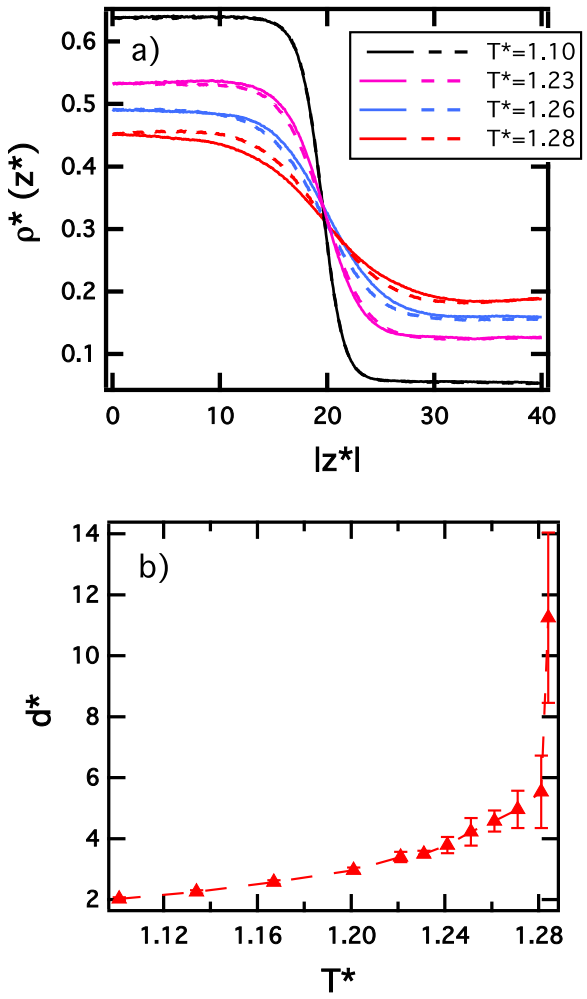

FIG. 3. (a) Superimposition of the density profiles of the LJ fluid at the liquid-vapor equilibrium calculated at four reduced temperatures. The left-hand sides of the density profiles are represented by solid lines and the right-hand sides by dotted lines; (b) calculated interfacial thickness at different reduced temperatures. The profiles and thickness of the interface are calculated with the Janeček method with a reduced cutoff of $r_c^* = 6.43$.

The profiles of the difference between the normal and tangential components of the pressure tensor calculated at $T^* = 1.10$ and 1.23 in Fig. 4(a) show similar features than those calculated at lower temperatures:[16,43] the peaks at the interfaces are symmetrical and are due to the non-zero tangential component of the pressure. The bulk regions do not contribute to this profile. The profile of $\gamma^*(z^*)$ shows that the contribution to the surface tension is the same for the two interfaces. For $T^* = 1.23$, as expected in this region, the peaks of the $p_N^*(z^*) - p_T^*(z^*)$ profiles are much less marked. However, they are observable and they show that the mechanical equilibrium of the liquid-vapor interface is maintained. The profile of $\gamma^*(z^*)$ defined in Eq. (8) is well-defined producing an accurate value of surface tension. Interestingly as shown in Fig. 4(b), the profiles of $\gamma^*(z^*)$ differ significantly at higher temperatures. For $T^* = 1.26$, the profile of $\gamma^*(z^*)$ allows to identify two interfaces with a bulk liquid phase presenting a flat zone. However, for $T^* = 1.28$, it is much more difficult to distinguish the interface with a monotonic increase of the local surface tension. By using a cutoff of $r_c^* = 6.43$, the limit temperature we can simulate for an accurate calculation of the surface tension is $T^* = 1.26$. Additional simulations with a larger L_z^* dimension ($L_z^* = 134$) confirm these findings. The density profiles calculated with this larger L_z^* length are

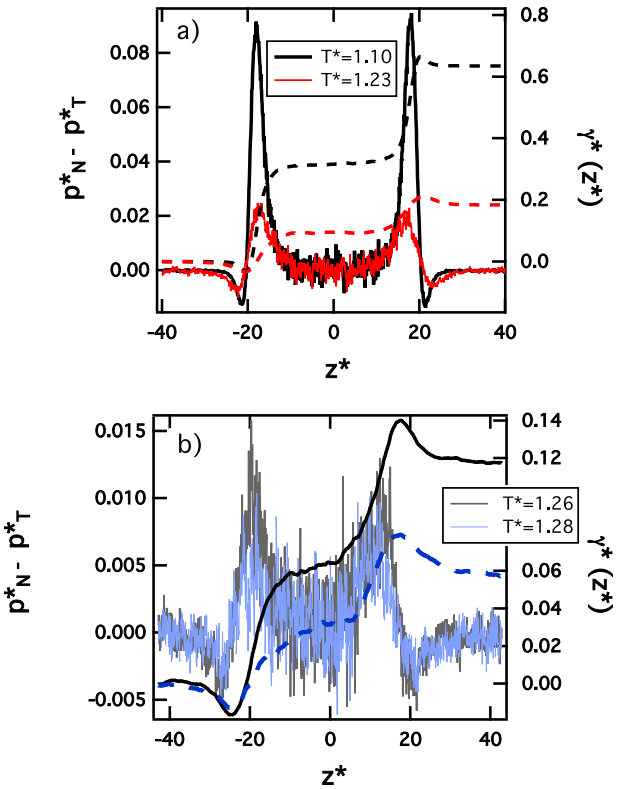

FIG. 4. Profiles of the difference $p_N^*(z^*) - p_T^*(z^*)$ and $\gamma^*(z^*)$ as a function of z^* for (a) $T^* = 1.10$ and 1.23 and (b) $T^* = 1.26$ and 1.28.

provided in the supplementary material with the profiles of $p_N^*(z^*) - p_T^*(z^*)$ and $\gamma^*(z^*)$.

We now focus on the cutoff-dependence of the liquid and vapor densities of the LJ fluid. Since we use smaller values of cutoff than $r_c^* = 6.43$, we only investigate the temperature range of [1.10–1.26] in order to develop a quantitative comparison.

These coexisting densities are calculated from simulations with both the Janeček approach and the truncated LJ potential with no long range correction of the energy used in the Markov chain. The reduced cutoff ranges from 3.21 to 6.43. In each case, we also report the values of coexisting densities calculated by Potoff and Panagiotopoulos using the grand canonical Monte Carlo (GCMC) simulations with the finite-size scaling (FSC) method.[33] The densities of the GCMC-FSC approach are calculated with the full LJ potential and long-range corrections are then performed with the method of Theodorou and Suter.[45] We also report in Appendix the liquid and vapor density calculated from intensive Gibbs Ensemble Monte Carlo (GEMC) simulations at different cutoffs.[36] The values of densities and surface tensions can be found in supplementary material.

Figs. 5(a) and 5(c) show the temperature dependence of the vapor and liquid densities calculated with the Janeček method. The coexisting densities calculated with the truncated LJ potential are shown in Figs. 5(b) and 5(d). Let us remind that at lower temperatures, $T^* = 0.67$ and 0.83 (see Ref. 16), we observed no cutoff-dependence of the liquid and vapor densities for $r_c^* \geq 3.75$ using the slab-based tail Janeček method and that a reduced cutoff of $r_c^* \geq 5.5$ is required to obtain the same accuracy with a truncated potential. All the curves presented here in Fig. 5 are for $T^* \geq 1.10$ which until now is the highest simulated temperature simulated using the two-phase methods.[6,7,16,30,43]

From Fig. 5, we observe that a reduced cutoff of $r_c^* = 3.21$ is unable to reproduce the coexisting densities in the critical region as compared with the GCMC-FSC method.[33] The differences between these two approaches increase with the temperature. However, the situation improves as r_c^* increases in the slab simulation. As already observed at low temperatures,[16] the slab-based tail Janeček approach mitigates the dependencies of the liquid and vapor densities on the cutoff radius compared to methods that do not use the long range corrections of the energy during the course of the simulation. However, a cutoff-dependence of the densities is observed, even with the Janeček approach, for $T^* > 1.20$.

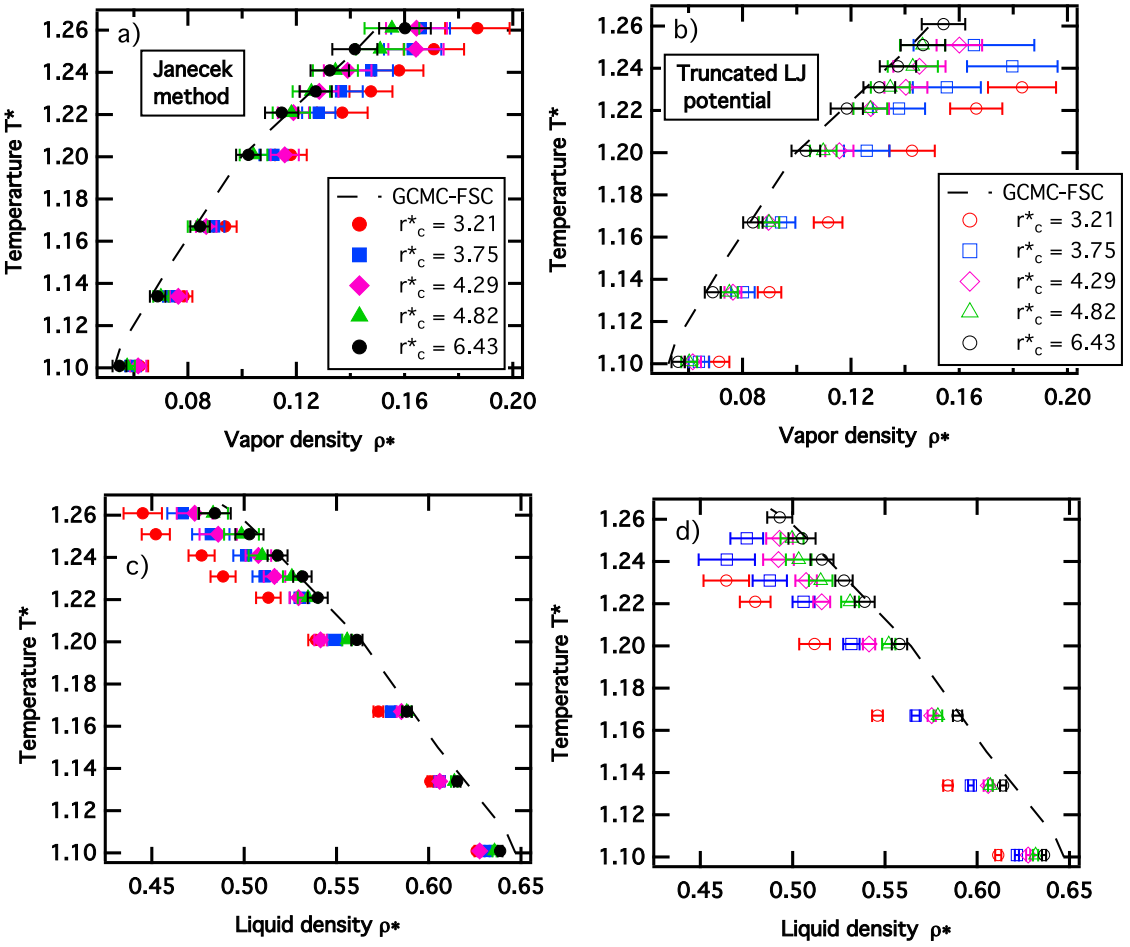

FIG. 5. Vapor (a) and (b) and liquid (c) and (d) densities calculated from the two-phase MC simulations at different reduced temperatures with both the slab-based tail Janeček method and the truncated Lennard-Jones potential model. The densities[33] calculated with the grand canonical Monte Carlo (GCMC) and the finite-size scaling (FSC) methods are given for comparison.

The relative differences between the coexisting densities calculated with the slab method with $r_c^* = 6.43$ and $r_c^* = 3.75$ defined by $\left[\rho^*(r_c^* = 6.43) - \rho^*(r_c^* = 3.75)\right]/\rho^*(r_c^* = 6.43)\right]$ is 0.4% (liquid) and 2.3% (vapour) at $T^* = 0.83$ with the Janeček approach. At $T^* = 1.24$, these deviations increase to 3.3% (liquid) and 12% (vapor) with the slab-based tail correction and to 10% (liquid) and 31% (vapor) with the truncated LJ potential.

To obtain good agreement with the densities calculated with the GCMC-FSC simulations in the temperature range of [1.10–1.24], we need a cutoff of $r_c^* = 6.43$. In this case, the results using either the truncated LJ potential or the slab-based tail method are very close: the relative differences between the densities calculated with the truncated potential and the Janeček technique are 0.4% for the liquid density and 2.7% for the vapor density. Nevertheless, with the Janeček approach, the use of a smaller cutoff of 4.82 offers quantitative agreement with the GCMC simulations with deviations of 2.8% (liquid) and 4% (vapor) at the highest temperature $T^* = 1.26$ reported here.

Increasing the cutoff value in slab simulations leads to a decrease of the vapor density and to an increase of the liquid density making then the phase diagram of the LJ fluid wider and closer to that calculated by the GCMC-FSC method. This cutoff-dependence on the density is mitigated through the use of the Janeček approach. Considering the recent GEMC simulations,[36] increasing the cutoff radius also improves the agreement with the densities calculated by the GCMC-FSC method but makes the phase envelope narrower.

The vapor pressures calculated by the GEMC and slab simulation methods are reported in the Appendix. They are calculated with $r_c^* = 8.0$ and $r_c^* = 6.43$ for the GEMC and slab MC methods, respectively. The GEMC methods are able to provide vapor pressures at higher temperatures compared to slab MC simulations but the Antoine fits show excellent agreement between the different approaches.

The surface tension calculated with the Janeček approach and the truncated LJ potential has also been calculated in the critical region. The surface tensions sum the intrinsic and long range corrections parts and are reported in Fig. 6 at different cutoff values. For the smallest cutoff used here ($r_c^* = 3.21$), the long range correction to the surface tension represents 34% of the total surface tension at $T^* = 1.1$ and 30% at $T^* = 1.26$. For the largest cutoff used here ($r_c^* = 6.43$), the tail correction contributes to 10% of the total surface tension at $T^* = 1.10$ and 13% at $T^* = 1.26$. The long range correction does not exceed 30% of the total surface tension in the critical region for a moderate cutoff. It can be reduced to 10% with a large cutoff radius. For the same cutoff, the percentage contribution of long range correction to the surface tension in the critical region is the same as that calculated at lower temperature on the orthobaric curve.

In the case of simulations using a cutoff $r_c^* = 6.43$, the two-phase simulations are able to model a liquid–vapor interface up to a reduced temperature of 1.26 with a very small surface tension ($\gamma^* = 0.044$) of the order of magnitude of the statistical fluctuations. Fig. 6(a) shows no cutoff-dependence

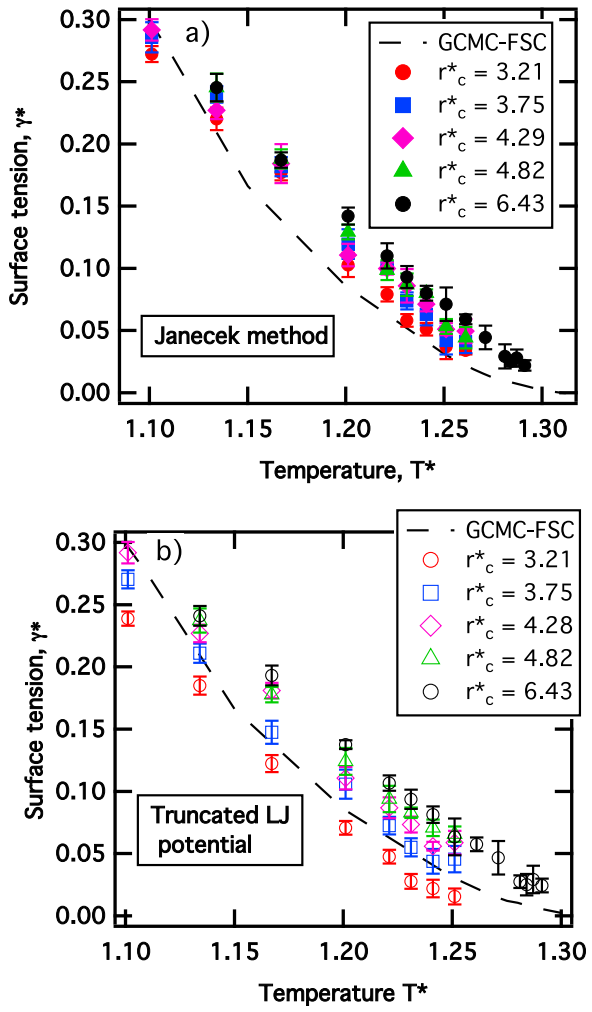

FIG. 6. The reduced surface tensions calculated in the critical region at different values of cutoff radius (r_c^*) using the Janeček approach and the standard truncated LJ potential. The surface tensions[33] calculated with the GCMC-FSC methodology are given for comparison.

at $T^* = 1.1$ with the Janeček approach whereas a dependence of the surface tension on the cutoff is shown in Fig. 6(b) at this temperature with the truncated LJ potential. With increasing temperatures in the critical region from $T^* = 1.20$, a dependence of the surface tension on the cutoff radius is observed with the Janeček method. The relative deviation between the surface tensions calculated at $r_c^* = 6.43$ and $r_c^* = 3.75$ increases from 0.2% ($T^* = 0.67$, see Ref. 16) to 15% ($T^* = 1.20$). A stronger dependence is then established in the case of the truncated LJ model for which the relative deviation increases up to 25% at $T^* = 1.20$.

We demonstrate that the use of a very large cutoff ($r_c^* = 6.43$) enables us to calculate the surface tension as we approach the critical point: the maximum temperature that we are able to simulate with the two-phase method is 1.26 ($\approx 0.97\,T_C^*$, where T_C^* was found to be 1.31 in Ref. 33). For $r_c^* = 6.43$, the results with the Janeček method and with the truncated potential are very close. The main advantage of the slab-based tail correction in the critical region is to reduce slightly the cutoff dependence of the surface tension. Concerning the deviations observed between the surface tensions calculated with the

two-phase and GEMC-FSC simulations, it is difficult to conclude.

One advantage of the two-phase simulation is to calculate density and pressure profiles in the critical region and this enables us to complete this study by representing some interfacial properties as a function of different powers of the distance $(T_C^* - T^*)$ from the critical point. For the study of these different scalings, we compare the data obtained with the GCMC-FSC approach[33] and the slab Monte Carlo simulations performed with the Janeček approach and a cutoff radius $r_c^* = 6.43$. First, we report the density difference between the liquid and vapor phases $(\rho_l^* - \rho_g^*)$ as a function of $(T_C^* - T^*)$ near the critical point in Fig. 7(a). We also add for comparison the density differences calculated from GEMC simulations[36] with $r_c^* = 8.0$. The difference in densities is expected to vanish at the critical point as $(\rho_l^* - \rho_g^*) \sim (T_C^* - T^*)^\beta$. The exponent β is equal to 1/2 in the van der Waals theory or mean-field theory[40,46] and to 0.32 in the critical-point theory and experiments.[40] The log-log plots of Fig. 7(a) give values of β equal to 0.33 ± 0.01 (GCMC-FSC), 0.31 ± 0.01 (GEMC), and 0.44 ± 0.01 (slab MC). The slab simulations provide a reasonable estimate of the critical exponent but are not as accurate as the GCMC-FSC and GEMC simulations. Indeed, the larger slope obtained with the slab simulations is explained by the fact that the differences in densities at the four highest temperatures are underestimated compared to those calculated by the GEMC and GCMC-FSC methods. However, as shown in Fig. 7(a) for lower temperatures in the near critical region, the three methods give the same scaling.

From the mean-field theory, the surface tension vanishes on approaching the critical point according to $\gamma^* \sim (T_C^* - T^*)^\mu$, where the critical-point exponent $\mu = 3/2$ in the mean-field theory[40] and $\mu = 1.26$ in the critical-point theory and experiments.[32,33,40,47] Fig. 7(b) shows the log-log plot of the surface tension versus $(T_C^* - T^*)$. The linear regression of the data gives a slope μ of 1.45 ± 0.04 (GCMC-FSC) and of 1.12 ± 0.02 (slab MC). The value of μ calculated from our MC simulations is closer to the value of 1.26[32,33,40,47] whereas the GCMC-FSC approach provides a value in agreement with previous simulations.[32,33]

Finally in Fig. 7(c), we report the interfacial thickness d^* as a function of $(T_C^* - T^*)$. The thickness of the interface d^* is calculated from the density profile fitted by a hyperbolic tangent function. The width of the interface is expected to diverge at the critical point as $d^* \sim (T_C^* - T^*)^\nu$. The linear regression of the interfacial thickness calculated from Monte Carlo simulations leads to a slope $\nu = -0.52 \pm 0.02$ whereas the mean-field theory[40] predicts $\nu = -1/2$ and the critical-point theory $\nu = -0.63$.[40] The slab-based tail Janeček approach used in MC simulations in the critical regions provides critical-point exponents β, μ, and ν that are between the typical values of the classical mean-field theory and of the critical-point theory and experiments indicating, however, that the dependencies of the different properties such as density, surface tension, and interfacial thickness on the temperature are well-reproduced near the critical point demonstrating that the slab simulations provide reasonable estimates of the critical scaling in the critical region.

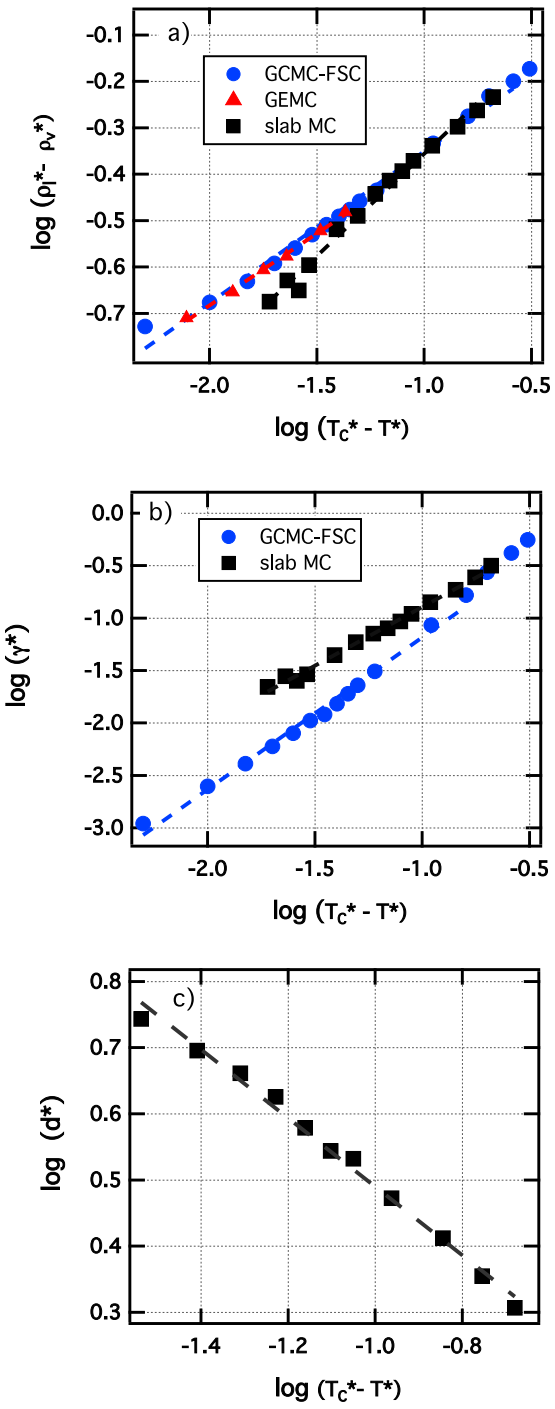

FIG. 7. (a) Log-log plot of the density differences $(\rho_l^* - \rho_g^*)$ versus $(T_C^* - T^*)$. The linear regression slopes are 0.33 ± 0.01 (GCMC-FSC), 0.31 ± 0.01 (GEMC) and 0.44 ± 0.01 (slab MC). (b) Log-log plot of the reduced surface tension γ^* versus $(T_C^* - T^*)$. The log-log plots give slopes $\mu = 1.44 \pm 0.04$ (GCMC-FSC) and $\mu = 1.12 \pm 0.02$ (slab MC); (c) Log-log plot of the interfacial width d^* as a function of $(T_C^* - T^*)$. The slope ν is equal to −0.52 ± 0.02 with the MC calculations. The dotted lines represent the least-squares fits to the different data. The interfacial widths for temperatures greater than 1.28 are not considered due to the difficulty of calculating them. The slab MC points are obtained with the Janeček approach and a cutoff radius $r_c^* = 6.43$.

IV. CONCLUSIONS

It is now well-established that the slab-based tail methods[16,17,31,43] that correct the configurational energy by adding long range corrections during the course of the

simulations enables us to obtain a surface tension independent of the cutoff from $r_c^* > 3$. For the coexisting densities, we need a larger cutoff of $r_c^* > 4$. All these studies[10,16,31] were performed at moderate temperatures ($<0.85\,T_C^*$).

In this paper, we have investigated the behaviour of the two-phase simulations to approach the critical point. We have examined the cutoff dependence on the coexisting densities and on the surface tension with the Janeček technique. We have compared these dependencies with those obtained for the truncated LJ potential with no long range corrections included during the simulation. We have taken great care to obtain well-converged density and pressure profiles in order to extract accurate values of surface tension and densities.

Firstly, a value of $r_c^* = 3.21$, which is commonly used in molecular simulations, leads to densities and surface tensions that deviate significantly from the results obtained from the grand canonical Monte Carlo simulations. In addition, we observe a strong cutoff-dependence of the surface tension and densities even with the Janeček approach. Secondly, we show that it is possible to approach the values of densities of the GEMC-FSC and GEMC simulations in the critical region but the price to be paid is to use a large cutoff, $r_c^* = 6.43$. For such a value, we do not observe any difference between the slab-based tail method and the truncated LJ potential in our two-phase simulations approaching the critical point up to $0.97\ T_C^*$. However, the improvements obtained using Janeček methods in the critical region are much less dramatic than observed at moderate temperatures ($<0.85\,T_C^*$).

Unlike the two-phase simulations, the GCMC-FSC approach cannot be used at temperatures below $0.7\ T_C^*$. However, the two-phase simulation method remains cutoff-dependent in the critical region [1.10–1.28] leading to surface tensions, coexisting densities, critical temperature, and densities that may change with the cutoff radius. However, the slab geometry method can be used with confidence up to $0.97\ T_C^*$ (*i.e.*, $\approx T^* = 1.26$) on condition of using a large cutoff of $r_c^* = 6.43$.

Finally, the Monte Carlo simulations carried out with the slab-based tail Janeček method with a large cutoff of $r_c^* = 6.43$ quantitatively reproduce the different dependences of the density, surface tension, and width of the interface on the temperature near the critical point.

SUPPLEMENTARY MATERIAL

See the supplementary material about the values of coexisting densities and surface tensions calculated at different cutoff radius and the density and surface tension profiles obtained with a larger box size.

APPENDIX A: COEXISTING DENSITIES CALCULATED FROM GEMC SIMULATIONS

For comparison, we report in Fig. 8 the vapor and liquid coexisting densities calculated using the GEMC method for large-system sizes and different cutoffs.[36] We observe that the GEMC simulations with $r_c^* = 8.0$ give an excellent agreement with the densities calculated by the GCMC-FSC approach. We note a cutoff dependence on the coexisting densities calculated with the GEMC method that simulates two distinct homogeneous boxes.

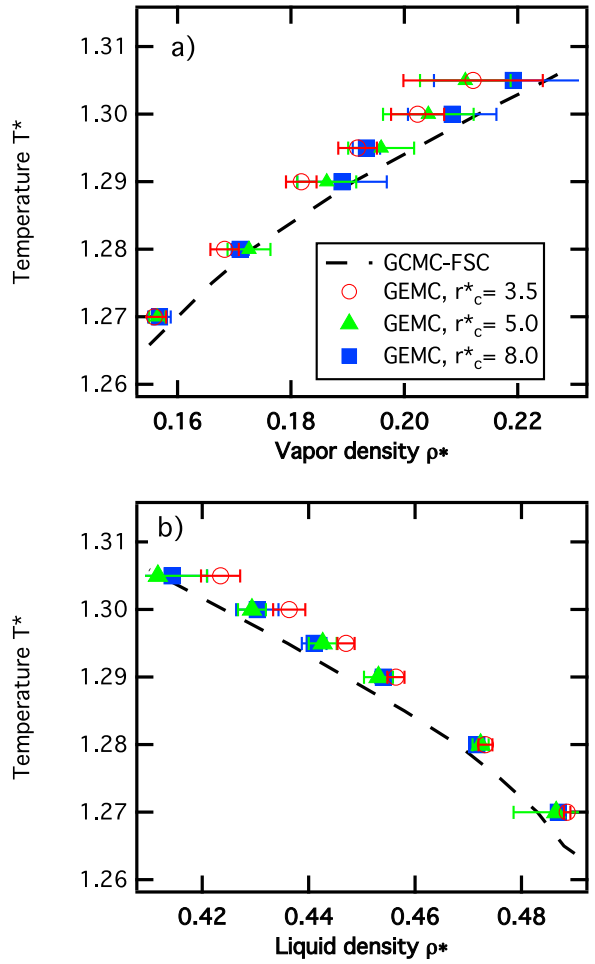

FIG. 8. Comparison between the (a) vapor and (b) liquid densities calculated with the GCMC-FSC[33] and GEMC[36] simulations.

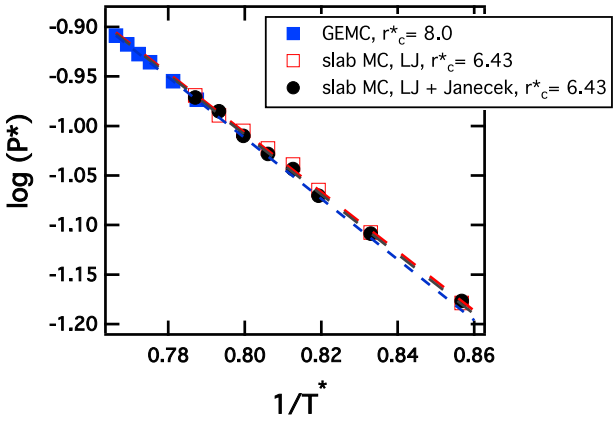

FIG. 9. Clausius-Clapeyron plots of the logarithm of the saturated vapor pressure as a function of the inverse temperature. For the GEMC simulations, we report the vapor pressure calculated with $r_c^* = 8.0$. For the slab simulations, the vapor pressures are calculated with $r_c^* = 6.43$ by using the truncated LJ potential and the Janeček approach. The dotted lines show the Antoine fits.

APPENDIX B: SATURATED VAPOR PRESSURES

The vapor pressure represented in Fig. 9 calculated from the slab simulations is compared with those obtained with the GEMC method. The vapor pressures of the slab simulations are obtained from the normal and tangential components of the pressure tensor calculated in the vapor regions by using the Irving and Kirkwood definition.

[1]K. S. Liu, J. Chem. Phys. **60**, 4226 (1974).
[2]J. K. Lee, J. A. Barker, and G. M. Pound, J. Chem. Phys. **60**, 1976 (1974).
[3]G. A. Chapela, G. Saville, and J. Rowlinson, Discuss. Faraday Soc. **59**, 22 (1975).
[4]M. Rao and D. Levesque, J. Chem. Phys. **65**, 3233 (1976).
[5]G. A. Chapela, G. Saville, S. M. Thompson, and J. S. Rowlinson, J. Chem. Soc., Faraday Trans. 2 **73**, 1133 (1977).
[6]M. Guo and B. Lu, J. Chem. Phys. **106**, 3688 (1997).
[7]A. Trokhymchuk and J. Alejandre, J. Chem. Phys. **111**, 8510 (1999).
[8]F. Goujon, P. Malfreyt, J. M. Simon, A. Boutin, B. Rousseau, and A. H. Fuchs, J. Chem. Phys. **121**, 12559 (2004).
[9]G. J. Gloor, G. Jackson, F. J. Blas, and E. de Miguel, J. Chem. Phys. **123**, 134703 (2005).
[10]J. Janeček, J. Chem. Phys. **131**, 6264 (2006).
[11]A. Ghoufi and P. Malfreyt, Phys. Rev. E **83**, 051601 (2011).
[12]J. C. Neyt, A. Wender, V. Lachet, and P. Malfreyt, J. Phys. Chem. B **115**, 9421 (2011).
[13]F. Biscay, A. Ghoufi, and P. Malfreyt, J. Chem. Phys. **134**, 044709 (2011).
[14]F. Biscay, A. Ghoufi, V. Lachet, and P. Malfreyt, J. Phys. Chem. C **115**, 8670 (2011).
[15]P. Malfreyt, Mol. Simul. **40**, 106 (2014).
[16]F. Goujon, A. Ghoufi, P. Malfreyt, and D. J. Tildesley, J. Chem. Theory Comput. **11**, 4575 (2015).
[17]A. Ghoufi, P. Malfreyt, and D. J. Tildesley, Chem. Soc. Rev. **45**, 1387 (2016).
[18]P. Orea, J. Lopez-Lemus, and J. Alejandre, J. Chem. Phys. **123**, 114702 (2005).
[19]M. Gonzalez-Melchor, P. Orea, J. Lopez-Lemus, F. Bresme, and J. Alejandre, J. Chem. Phys. **122**, 094503 (2005).
[20]J. R. Errington and D. A. Kofke, J. Chem. Phys. **127**, 174709 (2007).
[21]F. Biscay, A. Ghoufi, F. Goujon, V. Lachet, and P. Malfreyt, J. Chem. Phys. **130**, 184710 (2009).
[22]S. Werth, S. V. Lishchuk, M. Horsch, and H. Hasse, Phys. A **392**, 2359 (2013).
[23]J. Lopez-Lemus and J. Alejandre, Mol. Phys. **100**, 2983 (2002).
[24]C. Ibergay, A. Ghoufi, F. Goujon, P. Ungerer, A. Boutin, B. Rousseau, and P. Malfreyt, Phys. Rev. E **75**, 051602 (2007).
[25]A. Ghoufi and P. Malfreyt, Mol. Phys. **104**, 2929 (2006).
[26]E. Salomons and M. Mareschal, J. Phys.: Condens. Matter **3**, 9215 (1991).
[27]E. M. Blokhuis, D. Bedaux, C. D. Holcomb, and J. A. Zollweg, Mol. Phys. **85**, 665 (1995).
[28]F. Goujon, P. Malfreyt, A. Boutin, and A. H. Fuchs, J. Chem. Phys. **116**, 8106 (2002).
[29]F. Goujon, P. Malfreyt, and D. J. Tildesley, ChemPhysChem **5**, 457 (2004).
[30]V. K. Shen, R. D. Mountain, and J. R. Errington, J. Phys. Chem. B **111**, 6198 (2007).
[31]J. M. Míguez, M. M. Piñeiro, and F. J. Blas, J. Chem. Phys. **138**, 34707 (2013).
[32]J. E. I. Hunter and W. P. Reinhardt, J. Chem. Phys. **103**, 8627 (1995).
[33]J. J. Potoff and A. Panagiotopoulos, J. Chem. Phys. **112**, 6411 (2000).
[34]J. R. Errington, J. Chem. Phys. **67**, 012102 (2003).
[35]K. Binder, Phys. Rev. A **25**, 1699 (1982).
[36]M. Dinpajooh, P. Bai, D. A. Allan, and J. I. Siepmann, J. Chem. Phys. **143**, 114113 (2015).
[37]M. Fitzgerald, R. R. Picard, and R. N. Silver, Europhys. Lett. **46**, 282 (1999).
[38]J. G. Kirkwood and F. P. Buff, J. Chem. Phys. **17**, 338 (1949).
[39]J. H. Irving and J. Kirkwood, J. Chem. Phys. **18**, 817 (1950).
[40]J. S. Rowlinson and B. Widom, *Molecular Theory of Capillarity* (Clarendon Press, Oxford, 1982).
[41]J. P. R. B. Walton, D. J. Tildesley, J. S. Rowlinson, and J. R. Henderson, Mol. Phys. **48**, 1357 (1983).
[42]J. P. R. B. Walton, D. J. Tildesley, J. S. Rowlinson, and J. R. Henderson, Mol. Phys. **50**, 1381 (1983).
[43]F. J. Martinez-Ruiz, F. J. Blas, B. Mendiboure, and A. I. M.-V. Bravo, J. Chem. Phys. **141**, 184701 (2014).
[44]M. P. Allen and D. J. Tildesley, *Computer Simulation of Liquids* (Clarendon Press, Oxford, 1987).
[45]D. N. Theodorou and U. W. Suter, J. Chem. Phys. **82**, 955 (1985).
[46]J. W. Cahn and J. E. Hilliard, J. Chem. Phys. **28**, 258 (1958).
[47]A. M. Ferrenberg and D. P. Landau, Phys. Rev. B **44**, 5081 (1991).